Calibration of *HST* WFPC Images for Quantitative Analysis of Faint Galaxy Images

Kavan U. Ratnatunga[1], Richard E. Griffiths[1], Stefano Casertano[1]
Lyman W. Neuschaefer[1] and Eric W. Wyckoff[1]

Abstract

Accurate *V* and *I* flat fields for the Hubble Space Telescope Wide Field Camera have been obtained using the sky background in images taken for the Medium-Deep Survey, a Key Project. These super-sky flat fields have pixel-to-pixel rms variations of about 2.2 percent in *V* and 2.4 percent in *I* and are uniform to better than 3 percent peak-to-peak over almost all the exposed area. Super-sky flat fields can increase photometric accuracy of WFC images by about a factor of 3 with respect to Earth flats and because of the low level of illumination are better suited for quantitative study of faint images in deep exposures.

I. Introduction

The pipeline calibration established by the STScI for Wide Field and Planetary Camera (WFPC) images (MacKenty et al., 1992b) addresses the needs of the majority of primary observers, who typically have small observation sets with well exposed images for their targets of interest. The Medium Deep Survey (MDS) Key Project (Griffiths, et al., 1993) includes observations of a large number of random fields extending over multiple years and focuses on the properties of the faintest measurable objects found serendipitously. Accordingly, much effort in the early stages of the MDS project has been devoted to improving upon the pipeline calibration and selecting the optimum set of procedures to minimize observational errors. This is particularly important for quantitative analysis of faint extended sources with low signal-to-noise ratio.

While a primary (non-WFPC) observation executes a long uninterrupted integration, up to 40 minutes of parallel observation time are often available during each *HST* orbit. Noise in these observations is typically dominated by the CCD read noise: even for the longest single-orbit observations, the Poisson noise from the photon counts in the sky background contributes less than the read noise. In order to minimize the total noise and to improve the efficiency of scheduling parallel observations for the MDS, each orbit is used for a single WFPC exposure, between 20 and 40 minutes in duration, taken with the F785LP (*I*) or the F555W (*V*) filters. In a few cases, over 10 exposures were taken towards a single pointing; these fields include the deepest WFPC exposures taken so far with *HST*. The images contain mainly background sky counts, and our goal is to extract information on the faint stars and galaxies present.

1. Johns Hopkins University, Baltimore, MD 21218

The STScI WFPC pipeline calibration is based on a sequence of operations (MacKenty et al., 1992a; and see this volume), each of which removes some image artifact at the price of introducing a certain amount of extra noise. Briefly, the observed image is first corrected for the Analog to Digital Converter (ADC) error (Lauer 1989) using a lookup table. Next, a bias level is subtracted, together with the expected dark current for the time between CCD erasure and readout. Finally, flux calibration is ensured by multiplying the image by the inverse of the instrument response (flat field).[1]

Bias, dark and flat field frames all contain some measure of noise. The STScI calibration frames were created with the overall goal of achieving a noise contribution below one ADU (Analog-Digital Unit), which is smaller than the typical single-exposure read noise (about two ADU). However, if, as in the case of many MDS fields, several exposures with the same pointing are combined to reduce the image noise, the calibration noise does not decrease in the same way, since the same transformations are applied to each image in the stack. Therefore the noise introduced by the standard calibration process may dominate the total noise if more than three exposures with the same pointing are combined. Similarly, any systematic problems in the calibration, such as the gradients in the flat field that have been reported by Phillips et al. (1993, and this volume), will not be reduced and will become more significant in the presence of a smaller level of noise.

Because of the MDS focus on the quantitative study of the faintest observable objects, we have aimed our calibration strategy at achieving the lowest noise level possible, while at the same time improving the stability of the process and the photometric accuracy of our results. To this end, we have obtained new dark, bias, and flat field frames, taking into account possible time variations in each, and also additional corrections for the Charge Transfer Efficiency error. As a result, we have reduced the calibration-induced noise by 0.3 mag and the variation in the CCD response by a factor of at least 3.

In this contribution we discuss in detail our new super-sky flat fields, which are perhaps of general use. The other steps in our calibration strategy are discussed in a companion paper (Ratnatunga et al., 1993). The super-sky flat fields have been obtained using the sky background in a large number of MDS images, and appear to be essentially free from the problems found in Earth and internal flats, such as large-scale gradients, streaks, and other sharp features. At the same time, because they have been obtained at count rates similar to our science data, there is no concern about variations in the pixel-to-pixel response of the camera between high and low levels of illumination. These flat fields are substantially more uniform on both small and large scales than those obtained in the pipeline calibration, and allow much more accurate photometry even for faint objects.

1. A comprehensive review of these steps and the errors associated with the calibrations is given in the article by Biretta in this volume.

II. The Super-Sky Flat Field

a) Sky Background vs. Bright Earth Images

The standard pipeline approach to flat fields is to obtain exposures of the bright Earth as the *HST* field of view streaked across it (MacKenty et al., 1992a). These have the advantage of very low photon noise, because of the large signal accumulated in a short time. At the same time, they present several potential problems, especially for our goal of obtaining accurate photometry of faint objects.

First, the surface brightness of the Earth is not constant; as the spacecraft moves during the exposure, this produces streaks at a characteristic angle. The streaks can to some extent be removed via software developed by the WFPC IDT (Faber 1991). An improved version of this software has been implemented in STSDAS. In the IDT version of the software, some of the image processing was done with integer computations, which left a residual pattern identified by Phillips et al. (1993) using a subset of the MDS F785LP images. This problem was completely resolved by restacking the original Earth flats with the STSDAS version of the software. In some cases, however, the number of streaked flats available is insufficient for proper removal of the streaks, especially if the streak angles are similar.

Second, the surface brightness of the Earth is so high that the signal has to be reduced somehow to avoid saturation in the wide filters even in short exposures. For the F555W filters, for example, this has been achieved by coupling it with the F122M filter; the latter has a red leak that acts as a neutral-density filter, with an effective signal reduction of about 8 magnitudes. However, it is now apparent that the red leak is not uniform across the field of view; this introduces variations of up to 30 percent (peak-to-peak) in the system throughput. For the F785LP filter, flats created with and without the F122M filter are significantly different, which confirms that the latter filter is at least partly responsible for the problems.

Third, large doughnut-like features are seen, particularly in the *V*-band (MacKenty et al., 1992b, Hsu and Ritchie 1993); these appear to be images of the secondary mirror assembly, due either to pinholes in the filter or to back-reflected light.

The net result of these problems is the existence of severe problems in the flat fields, including large gradients and large-scale non-uniformities (of order 10–15 percent in each chip) and other sharp features such as doughnuts, all of which become apparent as (artificial) variations of the sky background when the flat fields are applied to sufficiently deep exposures. Some of these problems have already been pointed out and partly corrected by Phillips et al. (1993) using the first set of MDS exposures.

Another, more fundamental problem which may specifically affect faint images is that the back-illuminated CCDs in the WFPC are prone to quantum efficiency hysteresis effects (Janesick et al., 1985; Griffiths 1985). The camera was UV-flooded at the end of 1990, and during the course of the subsequent *HST* safings and decontamination episodes, the CCDs may have experienced some loss of the charge introduced by the solar UV-flood: this loss is highly non-uniform, with the corners of the CCDs and small, protruding areas on the CCD surfaces losing charge more rapidly than other areas. The effective QE in these areas, as measured in the Earth

flat with a high level of illumination, can be quite different from the effective QE for the low-level illumination present during the MDS observations. Consequently, in those areas, the Earth flats are not directly applicable to the faint images in which we are most interested. Conversely, Earth flats may be more appropriate than ours for bright images with high signal levels.

b) Flat Fields from the Sky Background

The MDS team has used a completely different approach from Earth flats to measuring the pixel-by-pixel variation of instrumental response. We have taken advantage of the fact that a large fraction of our observations contain essentially uniform sky, with a few weak sources scattered randomly across the field. This allows us to build a super-sky flat from the data themselves (see, e.g., Tyson 1990). The basic assumption is that the background sky level is spatially constant through each observation, once individual objects have been removed. This obviates both of the main problems with the earth flats, since no additional filter is required, and the flats are obtained from observations at the same count levels as our science data.

Ideally, the super-sky flats should be assembled from data taken with the camera under constant environmental conditions, i.e. at the same level of contamination of the field-flattening lenses covering the CCDs. Frames accumulated in Cycle 2 between 08/08/92 and 08/02/93 approximately meet this criterion. Care has been taken to ensure that the fields selected for the super-sky flats did not include data frames for which the background had a high level of scattered earthlight (recognized by their high absolute levels and shadowing caused by mirror support structures).

Although approximately constant in each observation, the sky background does vary from observation to observation, depending on ecliptic latitude, Sun Angle and average Earth Limb Angle. Different observations need to be scaled to a common mode with appropriate weights. For this purpose, we had to modify the STSDAS COMBINE task, in which we found a multitude of serious and non-trivial errors which were especially problematic when combining and scaling images according to exposure time and/or mode.

The final stack used to determine the super-sky flat includes 79 frames for the F785LP filter and 56 frames for the F555W filter. No more than three images with the same pointing have been included in either stack. Since the images all have different pointings, at each pixel a clipping algorithm has been used to eliminate the high values, which could be due to cosmic rays or to astronomical objects. (Note that this process cannot generally be used with primary observations, which would be likely to contain target objects positioned preferentially at the center of a CCD or of the overall field.)

Table 1: Characteristics of Super-Sky Flat

Filter	F555W	F785LP
Images	56	79
Mean Exposure (sec)	1650	2350
Mean Counts (ADU)	18.2	18.8
Expected rms error (raw)	2.8%	3.3%
Measured rms error (raw)	3.1%	3.4%
Final measured rms error after combining with Earth flat	2.2%	2.4%

The mean properties of each flat field are tabulated in Table 1. With an average sky background of 18 ADU, and 50–80 independent frames, a major contributor in the noise of the final flat-fields is the noise in the calibration frames, especially the dark. After the improvements in our calibration procedures, we obtain a pixel-to-pixel variation of about 3.1 percent in *V* and 3.4 percent in *I*. The rms noise expected from read, dark, and other known sources of noise is 2.8 percent and 3.3 percent respectively, very close to the measured values; this indicates that there are no significant unexplained sources of noise.

Although these flats appear already much better than the Earth flats, there is still room for some improvement. The Earth flats, with their larger signal, have a lower fractional pixel-to-pixel variation on small spatial scales. We have attempted to use this valuable small-scale information by applying a simple filtering algorithm, in which each pixel value is determined by multiplying a smoothed version of the super-sky flat by a destreaked, flattened Earth flat. The final flat fields thus produced have an rms pixel-to-pixel variation of 2.2 percent in *V* and 2.4 percent in *I* (rms), and are free from all the artifacts present in the Earth flats, such as gradients, doughnuts, streaks. The quality of the pipeline flat fields can be gauged by flattening them with the higher-quality super-sky flats; the result is shown in Fig. 1 in the form of a contour map.

c) Photometric Zero Point

The removal of the large-scale gradient present in the pipeline flats also improves significantly the photometric quality of the WFC. We estimate that, after including all sources of error, photometry with the WFC can be accurate to about 0.03 mag over all four chips, edges and other obvious (small) defects excluded. Because systematic effects in the flat fields are reduced, there is no need for separate photometric zero-points for the four CCDs, which were required to compensate for the different responses assigned to different chips.

The best values for the zero points to be used with our super-sky flat fields are 22.84 ± 0.01 in the *V* band and 21.47 ± 0.02 in *I*. These values are in acceptable agreement with those obtained by Phillips et al. (1993) from a subset of MDS fields, and also with those derived by Freedmann et al. (1993).

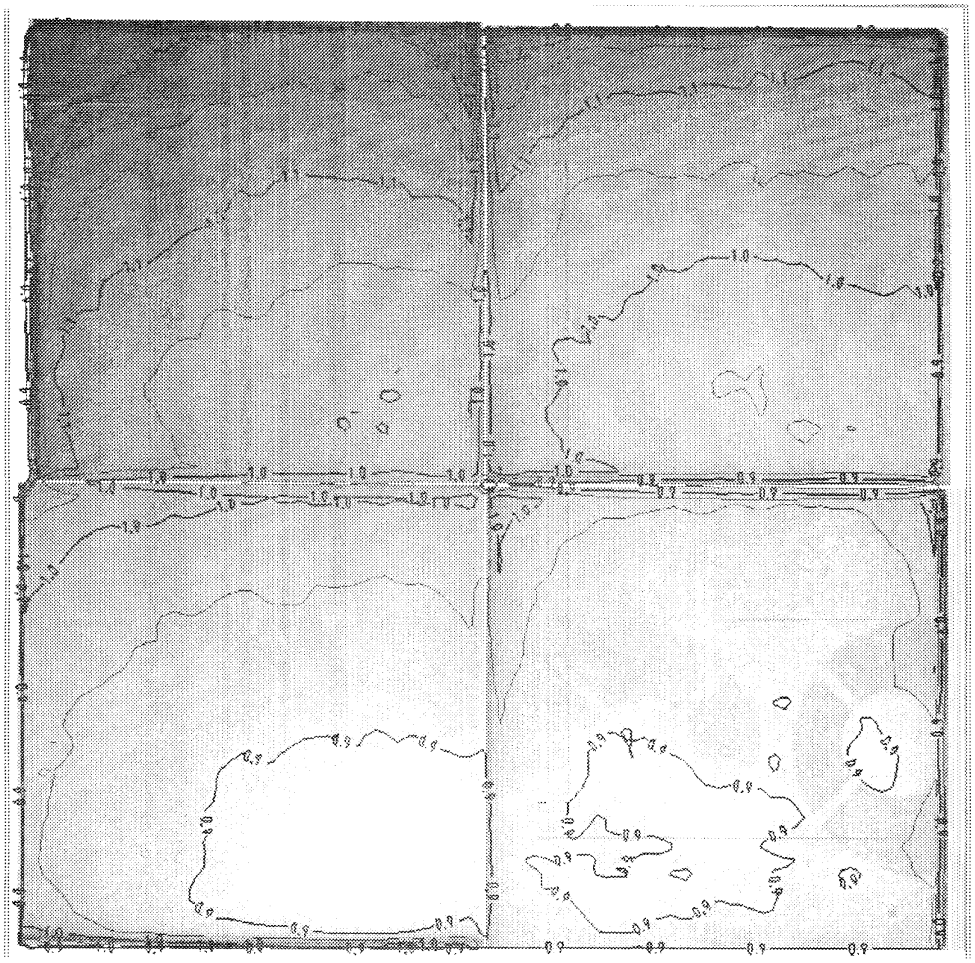

Figure 1: The large gradients and doughnuts in the pipeline F555W flat appear clearly when the pipeline flat is corrected with the super-sky flat.

d) Sky Brightness, Scattered Light, and Stacking of Images

Since super-sky flats are based on the assumption that the background sky brightness is constant across the field of view, special care must be exercised to ensure that no contamination from other sources of light is present. This includes large-scale variations from large nearby objects, such as bright galaxies (small objects in the field of view are excluded from the image-to-image comparison, and average out because of their random placement), scattered light, and gradients in the sky brightness itself.

The sky brightness depends on where the telescope is pointed. The main contributors to the background light are zodiacal, which depends on ecliptic angle, airglow, and scattered light, which depend on Sun angle and Earth limb angle. However, a change in overall sky brightness is benign for us, as long as the optical path through the telescope is the same, since it only offsets the image by a constant (after flat fielding). The concern would be a measurable gradient in the sky brightness in a single field, that is, over scales of order 3 arcmin.

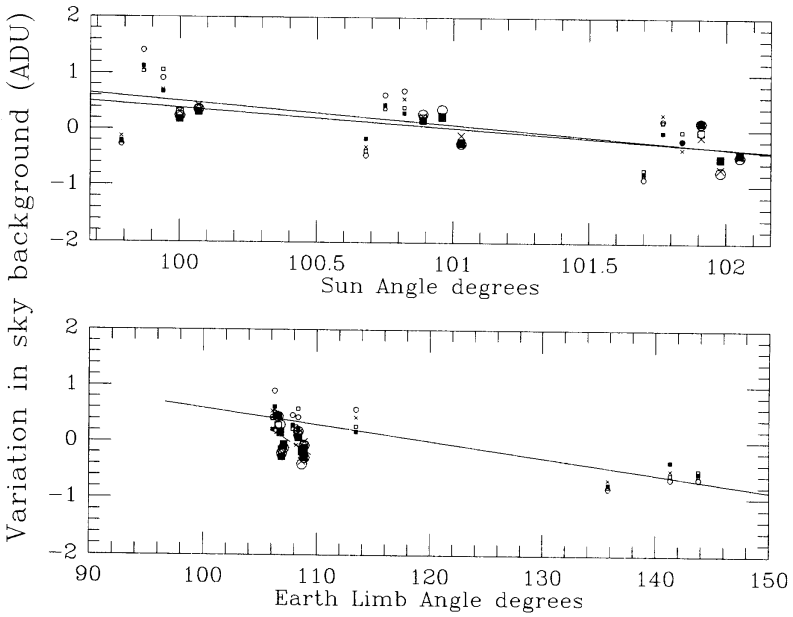

Figure 2: Change in the sky background among several observations of the MDS field near 3C273 in the three days of observation. The sky background level is determined in each exposure from the mode of the observation, separately for each CCD. Top: variation in sky background as a function of Sun angle. Bottom: residual as a function of Earth limb angle, after removal of a linear term in Sun angle. Within the 0.25 ADU precision of each measurement, the background is the same for all CCDs, indicating that any scattered light is distributed uniformly over the four chips and that any overall gradient is negligible.

We have attempted to put limits on any gradient in sky brightness in two different ways. First, we find no measurable variations in the sky brightness of individual images at the 1 percent level (peak-to-peak in 100-pixel squares), after reduction with our super-sky flats and object removal. This is the case even for images with very different sky background levels, including one taken at only 51° Sun angle which has a background 4 times higher than all others. Second, we have measured the change in the sky background among several observations of the MDS field near 3C273. In the three days of observation, the Sun angle increased from 100° to 102°. Most of the observations were taken at an average Earth limb angle of 105°, with some taken at 140°. The sky background level was determined in each exposure from the mode of the observation, separately for each CCD, with an error of 0.25 ADU (see Fig. 2). Within the precision of the measurement, the background is the same for all CCDs, indicating that any scattered light is distributed uniformly over the four chips and that any overall gradient must be small. Furthermore, the variations with Sun angle and Earth limb angle are small, consistent with 1 percent and 0.2 percent per degree respectively in this range. Both point at very small variations over the 3 arcmin scale of individual images. We conclude that, even if scattered light is present, as it almost certainly is, it is transmitted through the Optical Telescope Assembly just like all other light to a sufficiently good approximation (as far as our flats are concerned), and thus it introduces no adverse effect in either images or super-sky flats.

A final, related consideration concerns the stacking of images of the same field.

Coincidence routines, used to remove cosmic rays and other imperfections, typically rely on expecting the same signal at the same position. When the calibration is carefully conducted, the day-to-day variation in sky background is significant with respect to the noise, and therefore it must be corrected to avoid false rejections. At the same time, the typical sky level must be retained in order for the noise model to predict the image noise properly. Ideally, the measured signal should be used to determine the noise contribution from each image in the stack, while the corrected signal (flat-fielded and sky-subtracted) should be used in combining the images. Proper implementation of this method requires in principle retaining a separate noise image, which is not possible with current STSDAS software.

On the other hand, if all images in the stack have the same pointing, the flat-field correction can be applied after stacking, and an acceptable compromise is to correct images by a small additive constant to bring them to a common sky background. The mode offset option in the image combination tasks would be very effective for this purpose. Unfortunately, in their current (November 1993) incarnation, the relevant STSDAS tasks appear to suffer from several limitations, restrictions and bugs which have made our path fairly treacherous. We recommend careful evaluation, especially of issues of scale and weight calculation, combination of substacks, and proper noise model, before using the current STSDAS tasks. Even after removing existing bugs, the current incarnation of the image-combination software in STSDAS cannot properly deal with the stacking of overlapping images with different pointings, for which flat-field corrections must be applied before stacking, and therefore the information on the noise at each pixel is lost. A better program, which computes an error image as well as the combined image, is required for this case to be addressed properly.

III. Conclusions

Detection and quantitative study of faint objects in WFPC images is possible if the appropriate effort is put into the calibration process. The camera is sufficiently stable for good photometric performance (at the 3 percent level or better). However, especially for faint objects, calibration is an important source of both noise and systematic effects which have proved rather stubborn. In order to achieve a better performance in both sensitivity and photometric stability, we have augmented the standard STScI pipeline calibration with some additional procedures. Noise in the bias and dark frames has been reduced by judicious filtering, which includes removing known patterns and smoothing over scales where nothing but noise appears to be present.

A more significant improvement is given by the use of so-called super-sky flat field images, obtained from a combination of the sky background at many different pointings, instead of Earth flats. The latter suffer from streaks and non-linearity, and also from large-scale inhomogeneities at the 15–20 percent level which are difficult to eliminate. Super-sky flats are shown to be repeatedly flat at the 1 percent level over scales of several pixels, and are better-suited for faint objects because of the lower level of illumination compared with the Earth flats. Earth flats are useful in combination with super-sky flats to remove the high-frequency noise component to which the sky background, with its lower signal level, is more sensitive.

Our calibration procedures improve significantly both photometric accuracy and sensitivity for faint images. Photometric accuracy is 0.03 mag, or a factor of 5 better than that obtained with standard procedures, mainly because of the use of super-sky flat fields. Sensitivity is improved by about 0.3 mag, corresponding to about a factor 2 in observing time, thanks to the reduced noise in the calibration files, especially bias and dark.

The improved calibration files have been made available to the community through STEIS.

This work is based on observations taken with the NASA/ESA Hubble Space Telescope, obtained at the Space Telescope Science Institute, which is operated by the Associations of Universities for Research in Astronomy, Inc., under NASA contract NAS5—26555. Coordination and analysis of data for the Medium-Deep Survey is funded by STScI grants GO 2684.0X.87A and GO 3917.0X.91A. We acknowledge the helpful support of the STScI WFPC reduction team in acceding to our frequent requests for additional calibration data, and for extensive and illuminating discussions on various aspects of the calibration process.

References

Faber, S. M., et al, 1991, 'Final Orbital/Science Verification Report for the Wide Field and Planetary Camera'

Freedman, W. L., et al, 1993, preprint

Griffiths, R. E., 1985, Wide Field and Planetary Camera Instrument Handbook, version 1.0, STScI publication

Griffiths, R. E., et al., 1993, ApJ, submitted

Janesick, J., Elliott, T., Daud, T., McCarthy, J., and Blouke, M. M., 1985, Proc. S.P.I.E. 570, 46

Hsu, J. C., and Ritchie, C. E., 1993, Proc. S.P.I.E., in press

Lauer, T. R., 1989, PASP 101, 445

MacKenty, J. W., Sparks, W. B., Ritchie, C. E., and Baggett, S. M., 1992a, in 'Science with the Space Telescope,' eds. P. Benvenuti and E. Schreier, p. 595

MacKenty, J. W., et al., 1992b, 'Wide Field and Planetary Camera Instrument Handbook,' version 3.0, April 1992

Phillips, A. C., Forbes, D. A., Bershady, M. A., Illingworth, G. D., and Koo, D. C., 1993, AJ, submitted

Ratnatunga, K. U., Griffiths, R. E., Casertano, S., Neuschaefer, L. W., and Wyckoff, E. W., 1993, AJ, submitted

Tyson, A. J., 1990, in 'CCDs in Astronomy', A.S.P. Conference Series Vol. 8, ed. G. H. Jacoby, p. 1